Highly Dispersed Metal Nanoparticles in Functionalized SBA-15

Chia-min Yang, Pang-hung Liu, You-fu Ho, Chien-yang Chiu, and Kuei-jung Chao*

Department of Chemistry, National Tsinghua University, Hsinchu, 300, Taiwan

Received August 8, 2002. Revised Manuscript Received October 25, 2002

The preparation and characterization of highly dispersed metal nanoparticles in mesoporous silica SBA-15 are reported. The functionalization with organosilane to generate a monolayer of charged groups on the pore surface facilitates uniform distribution of ion-exchanged metal precursors in the channels of SBA-15, which, upon reduction, results in highly dispersed metal nanoparticles supported in SBA-15. Under mild reduction conditions, the surface functionality remains and so allows further metal incorporation cycles to achieve higher metal loading. After reduction in hydrogen flow, disk-shaped Pt nanoparticles in Pt/SBA-15 and spherical Au nanoparticles in Au/SBA-15 have been characterized in the channels of SBA-15 by PXRD, XAS, and TEM. Secondary Pt incorporation in Au/SBA-15 produces coexisting small Pt nanoparticles with large Au nanoparticles in the host channels. This preparation method is capable of template synthesis of various metal nanostructures with controlled morphology and composition inside the channels of mesoporous materials.

Introduction

Nanostructured materials represent a transition between the individual molecules and bulk solids, and have unique size-dependent catalytic, nonlinear optic, semiconductive, and magnetic properties.[1] These distinct properties may be attributed to the quantum confinement phenomena derived from the change in the density and effective band gap of the electronic energy level as well as a high ratio of surface to bulk atoms.[2] Therefore, selective synthesis of metal nanoparticles with specific size and shape would generate significant opportunities for applications.

Metal nanoparticles can be prepared via template, or so-called "host−guest" synthesis. The void dimension of host templates may confine the size and shape of the guest nanomaterials. Suitable templates include micelles of surfactants and polymers,[3,4] inversed microemulsions,[5] porous glasses,[6] porous carbon,[7] and molecular sieves.[8,9] The template-synthesized metal colloids or nanoparticles are either suspended in solution or supported on a solid. However, supported metal nanoparticles in porous host materials are more desired for practical applications. Mesoporous silicas (such as MCM-41[10] and SBA-15[11]) with ordered channel structures of pore diameters in the range of 1.5−30 nm and huge internal surface areas of 700−1000 m^2/g are suitable supports.

Recently, a novel method of preparing densely packed metal nanowires in MCM-41 and MCM-48 silicas with pore diameters of 2−3 nm has been demonstrated.[12] A monolayer of charged organic groups attached on the pore surface of mesoporous silica can adsorb and interact strongly with oppositely charged metal precursors, resulting in a highly metal loaded composite in a single incorporation step. On the other hand, the morphology of metal nanostructures can be controlled by tuning the pore structure of host mesoporous silica as well as the metal loading amount. In this study, the formation of highly dispersed metal nanoparticles in functionalized mesoporous silica SBA-15 has been characterized. SBA-15 silica has thick pore walls (3.1−6.4 nm) and larger pore size (in the range of 4.6−10.0 nm) than that of MCM-41 and MCM-48,[11] which may facilitate the diffusion of relative bulky molecules and

* To whom correspondence should be addressed. Phone: 886-3-571-5131 or 3377. Fax: 886-3-572-0964. E-mail: kjchao@mx.nthu.edu.tw.

(1) Schmid, G. *Clusters and Collids*; VCH: Weinheim, 1994.
(2) Alivisastos, A. P. *Science* **1996**, *271*, 933.
(3) (a) Pileni, M. P. *Pure Appl. Chem.* **2000**, *72*, 53. (b) Toshima, N. *Pure Appl. Chem.* **2000**, *72*, 317. (c) Selvan, S. T.; Spatz, J. P.; Klok, H.; Möller, M. *Adv. Mater.* **1998**, *10*, 132. (c) Bronstein, L.; Kramer, E.; Berton, B.; Burger, C.; Forster S.; Antonietti, M. *Chem. Mater.* **1999**, *11*, 1402.
(4) For a review see: Nagy, J. B.; Hannus, I.; Kiricsi, I. In *Nanoparticles and Nanostructured Films;* Fendler, J. H., Ed.; Wiley-VCH: Weinheim, 1998; p 389.
(5) Dresco, P. A.; Zaitsev, V. S.; Gambino, R. J.; Chu, B. *Langmuir* **1999**, *15*, 1945.
(6) Justus, B. L.; Tonnucci, R. J.; Berry, A. D. *Appl. Phys. Lett.* **1992**, *61*, 3151.
(7) (a) Scardi, P.; Antonucci, P. L. *J. Mater. Res.* **1993**, *8*, 1829. (b) Joo, S. H.; Choi, S. J.; Oh, I.; Kwak, J.; Liu, Z.; Terasaki O.; Ryoo, R. *Nature* **2001**, *412*, 169.
(8) Wang, Y.; Herron, N. *J. Phys. Chem.* **1988**, *92*, 4988.
(9) (a) Sasaki, M.; Osada, M.; Sugimoto, N.; Inagaki, S.; Fukushima, Y.; Fukuoka, A.; Ichikawa, M. *Microporous Mesoporous Mater.* **1998**, *21*, 597. (b) Wang, L. Z.; Shi, J. L.; Zhang, W. H.; Ruan, M. L.; Yu, J.; Yan, D. S. *Chem. Mater.* **1999**, *11*, 3015. (c) Michalik, J.; Brown, D.; Yu, J. S.; Danilczuk, M.; Kim, J. Y.; Kevan, L. *Phys. Chem. Chem. Phys.* **2001**, *3*, 1705. (d) Jung, J. S.; Chae, W. S. McIntyre, R. A.; Seip, C. T.; Wiley, J. B.; O'Connor, C. J. *Mater. Res. Bull.* **1999**, *34*, 1353.
(10) Kresge, C.; Leonowicz, M.; Roth, W.; Vartuliand, C.; Beck, J. *Nature* **1992**, *359*, 710.
(11) (a) Zhao, D.; Feng, J.; Huo, Q.; Melosh, N.; Fredrickson, G. H.; Chmelka, B. F.; Stucky, G. D. *Science* **1998**, *279*, 548. (b) Zhao, D.; Huo, Q.; Feng, J.; Chmelka, B. F.; Stucky, G. D. *J. Am. Chem. Soc.* **1998**, *120*, 6024.
(12) Yang, C. M.; Sheu, H. S.; Chao, K. J. *Adv. Funct. Mater.* **2001**, *12*, 143.

10.1021/cm020822q CCC: $25.00
Published on Web 11/28/2002

the mobility of nanostructured metals. Propyltrimethylammonium chloride groups (−PTA$^+$Cl$^-$) are uniformly distributed in the channels of SBA-15 and are ion-exchanged with anionic metal complexes. Upon reduction in hydrogen flow, highly dispersed metal nanoparticles in SBA-15 are formed. Simultaneous incorporation of platinum and gold nanoparticles in SBA-15 is also reported.

Experimental Section

Materials Preparation. Siliceous SBA-15 was synthesized following the literature procedure.[11] A 4.0-g portion of triblock copolymer Pluronic P-123 template was dissolved with stirring in a solution of 30 g of water and 120 g of 2 N HCl at 313 K, and 8.5 g of TEOS was then added. The resulting mixture was stirred at 313 K for 20 h, and then was aged at 353 K for 2 days under static condition. The as-prepared sample was recovered by filtration and air-dried at 353 K overnight. The organic template was removed by calcination in air at 813 K for 6 h. Prior to surface functionalization, the calcined SBA-15 was refluxed in water for 1 h, followed by heating in a vacuum at 423 K to remove residual water. A 0.5-g aliquot of rehydrated SBA-15 was suspended in 100 mL of toluene, and 10 mL of *N*-trimethoxysilylpropyl-*N*,*N*,*N*-trimethylammonium chloride (TPTAC, 50 wt % in methanol, Gelest) was added. The mixture was stirred at room temperature for 12 h, which was followed by reflux at 353 K for 6 h. The TPTAC-functionalized SBA-15 (TPTAC−SBA-15) was washed with toluene and ethanol, and dried in air.

For metal incorporation, TPTAC−SBA-15 was mixed with the ethanol solution of H_2PtCl_6 or $HAuCl_4$. Because the electrostatic interaction between cationic PTA group and anionic metal precursor is strong, mixing for ∼10 min is sufficient to have fully ion-exchanged sample. The resulting Pt/SBA-15(s) and Au/SBA-15(s) samples were washed with ethanol, dried in ambient air, and then reduced in hydrogen flow at 373−573 K. The reduced composites of Pt/SBA-15 and Au/SBA-15 were optionally subjected to a secondary Pt incorporation/reduction cycle, with the same procedures as described above to form Pt−Pt/SBA-15 and Pt−Au/SBA-15 composites.

Characterization. Surface functionalization was monitored by Fourier transformation infrared spectroscopy (FTIR) using a Perkin-Elmer FTIR 1720X spectrometer, and by solid-state ^{29}Si MAS NMR spectrometry with a Bruker DSX400WB spectrometer and a commercial MAS probe. Compositions were obtained by ICP-AES analysis using a Jarrell-Ash-ICAP 9000 device.

Metal particle sizes and structures were characterized by X-ray absorption spectroscopic measurements (XAS), powder X-ray diffraction (PXRD), and transmission electron microscopy (TEM) with energy-dispersive X-ray analysis (EDX). In-situ XAS measurements were done in transmission mode on the Beamline BL17C of the Synchrotron Radiation Research Center (SRRC), Taiwan, with storage ring energy of 1.5 GeV and a beam current between 120 and 200 mA. PXRD patterns were collected on a Mac Science 18MPX diffractometer with Cu Kα radiation. TEM and EDX were carried out on a JEOL JEM-2010 electron microscope equipped with an Oxford EDX analysis system. Samples were embedded in resin and ultramicrotomed into slices with thickness of ∼50 nm for TEM and EDX investigations.

The pore diameter, pore volume, and surface area of the samples were derived from the nitrogen sorption isotherm at 77 K using a Micromeritics ASAP 2010 system. Prior to measurements, the sample was evacuated at 573 K for 12 h. The total pore volume was estimated from the amount adsorbed at a relative pressure (P/P_0) of about 0.95, whereas the surface areas were obtained from BET treatment of the isotherms in the P/P_0 range of 0.05−0.25. However, because SBA-15 contains micropores,[13] BET surface areas cannot be taken at face value but only as a comparison in a series of samples. The mesopore size distribution was calculated on the basis of desorption branches of nitrogen isotherms using the BJH method, and the surface and structural heterogeneity of mesopores was shown in the shape of adsorption hysteresis.

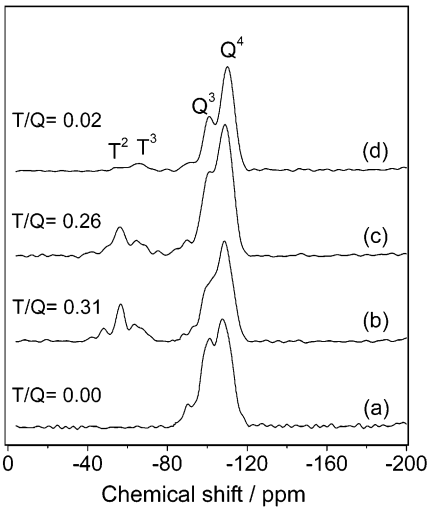

Figure 1. ^{29}Si NMR spectra of rehydrated SBA-15 (a), TPTAC−SBA-15 (b), and Pt/SBA-15 reduced at 423 K (c) and 573 K (d), respectively.

Results and Discussion

Functionalization of SBA-15 with TPTAC. PTA functional groups attached onto the pore surface of SBA-15 were confirmed by FTIR as that of siliceous MCM-41.[12] Upon functionalization, IR absorption intensity of silanol groups at 3750 cm^{-1} were observed to decrease with the appearance of absorption peaks of C−H bonds (2900−3000 cm^{-1}), C−N bonds (∼1490 cm^{-1}), and Si−C bonds (∼1250 cm^{-1}). TPTAC reacted with surface silanol groups in the channels of SBA-15 was also examined by Si NMR in this study. Solid-state ^{29}Si MAS NMR of the rehydrated, TPTAC-functionalized, and Pt-incorporated SBA-15s are shown in Figure 1. Distinct resonances can be observed for the siloxane [Q^n = Si−$(OSi)_n(OH)_{4-n}$, n = 2−4] and organosiloxane [T^m = R−Si−$(OSi)_m(OH)_{3-m}$, m = 1−3] species. The rehydrated SBA-15 possesses Q^3 and Q^4 peaks at around −100 and −111 ppm, respectively (Figure 1a). The Q^3 to Q^4 ratio (Q^3/Q^4) of ca. 0.8, indicates a high degree of coverage of silanol groups on the pore surface of rehydrated SBA-15. After functionalization with TPTAC, the intensity of Q^3 peak decreases (Q^3/Q^4 ∼ 0.5), accompanied by the appearance of T^2 and T^3 peaks centered at around −57 and −65 ppm, respectively on TPTAC−SBA-15 (Figure 1b).

The relative integrated intensities of NMR signals of the organosiloxane (T^m) and siloxane (Q^n) (T/Q ratios) can be employed to estimate the incorporation amount of functional groups. On TPTAC−SBA-15, the T/Q ratio was ca. 0.31, implying high surface coverage of PTA groups. After anion-exchange with $PtCl_6^{2-}$ and hydrogen reduction at 423 K, the ^{29}Si MAS NMR spectrum of the composite still exhibited intense T^m peaks (Figure 1c) with T/Q ratio of ca. 0.26. That indicates most of the surface PTA groups remained after H_2 treatment at 423

(13) Kruk, M.; Jaroniec, M.; Ko, C. H.; Ryoo, R. *Chem. Mater.* **2000**, *12*, 1961.

K, and are available for further metal incorporation processes. When the metal was reduced at 573 K, almost all the attached PTA groups were decomposed, as indicated by the extremely low intensity of organosiloxane species (T/Q ∼ 0) (Figure 1d). This is in good agreement with the thermal analysis of TPTAC−SBA-15, which shows that the decomposition temperature of PTA groups is ∼500 K under nitrogen flow.[12] Upon reductive formation of metal nanostructures in SBA-15 at low temperature, the surface-charged TPA groups can be preserved for further metal incorporation cycles, whereas under high-temperature reduction, they should be decomposed and removed from the channels of SBA-15.

In-Situ XAS Investigation of the Formation of Pt/SBA-15. Pt nanoparticles were formed from Pt/SBA-15(s) by reduction in hydrogen flow at 573 K. The reduction and decomposition of the metal complexes in the composite were monitored by in-situ XAS measurements. The spectra were measured from 200 eV below the Pt L_{III}-edge (11564 eV) to 1200 eV above the edge, and standard Pt foil was used as reference for energy calibration as shown in Figure 2a. After reduction, the white line intensity decreased significantly, accompanied by a change of the shape of absorption profile, which indicates that the surface $PtCl_6^{2-}$ anions are decomposed to form metal nanoparticles. After air exposure, the white line intensity of Pt was found to increase slightly, which was even higher than that of the Pt foil standard. In addition, the absorption edge showed a slight shift toward the platinum oxide standard, indicating partial oxidation of Pt nanoparticles.

Fourier transform (FT) profiles of k^3-weighted Pt L_{III}-edge EXAFS and the curve fitting results are shown in Figure 2b and Table 1. The EXAFS of Pt/SBA-15(s) consists of a single peak of Pt−Cl (d = 2.33 Å) with coordination number (CN) of 6, which is identical to that of H_2PtCl_6. This suggests that the coordination, as well as the geometry, of ion-exchanged $PtCl_6^{2-}$ anions were not perturbed in the Pt/SBA-15(s) composite. After reduction, the EXAFS of Pt/SBA-15(r) mainly consists of a first-shell Pt−Pt peak (d = 2.77 Å, CN = 10.3). After exposure to air, the intensity of the Pt−Pt peak of Pt/SBA-15(a) composite was observed to be lower than that of Pt/SBA-15(r), accompanied by the appearance of the Pt−O peak (d = 2.01, CN = 1.0). The corresponding Pt−Pt coordination number was reduced from 10.3 to 7.5 as indicated in Table 1. The average size of Pt metal particles can be estimated from the Pt−Pt coordination number based on face-centered cubic Pt structure and a spherical model.[14] It has been found to decrease from 2.9 to 1.0 nm after air exposure, probably due to the oxidation of a distinct amount of surface Pt atoms of metal particles upon exposure to air. A plausible explanation for this phenomenon is that the Pt nanoparticles have a high percentage of surface Pt atoms and may not be spherical in shape.

TEM and PXRD Investigations of Pt/SBA-15. TEM investigation provides direct observation of the morphology and distribution of Pt nanoparticles in the Pt/SBA-15(a) composite. The typical TEM images of Figure 3 clearly show uniform and highly dispersed Pt

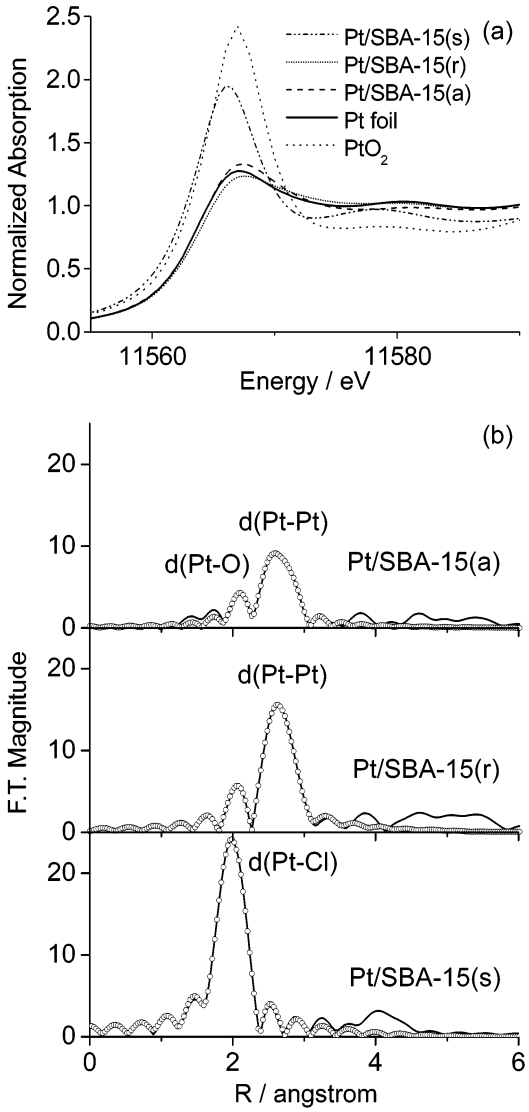

Figure 2. (a) Normalized Pt L_{III}-edge XANES of Pt/SBA-15 samples, Pt foil, and PtO_2 powder. (b) Fourier transforms of Pt L_{III}-edge k^3-weighted EXAFS data (−) and the fitted results (○), respectively, for Pt/SBA-15 samples. Note that the phase shifts were not corrected.

Table 1. Pt L_{III}-Edge EXAFS Results for the In-situ Experiment of Pt/SBA-15 Composite

sample	shell	R Å[a]	CN[a]	σ^2 10^{-3} Å^2	R factor 10^{-4}	particle size[b] nm
Pt/SBA-15(s)	Pt−Cl	2.33	6.2	2.8	0.2	
Pt/SBA-15(r)	Pt−Pt	2.77	10.3	6.0	6.5	2.9
Pt/SBA-15(a)	Pt−Pt	2.77	7.5	7.1	27	1.0
	Pt−O	2.01	0.9	7.8		

[a] Interatomic distance and coordination number. [b] Particle sizes were estimated from a spherical model with face-centered cubic Pt structure.

nanoparticles in the hexagonal channels of SBA-15. ICP−AES analysis reveals a Pt content of ∼8 wt % on Pt/SBA-15 higher than that (∼1.5−3 wt %) in Pt-loaded SBA-15 without rehydration prior to functionalization. The Pt particles are in the size range of 1.2−3 nm, generally not spherical, and almost exclusively stayed inside the channels of host SBA-15. The cross sectional image of the Pt/SBA-15(a) composite (Figure 3b) reveals the disk-shaped Pt nanoparticles attached, or "coated", on the hexagonal pore of host SBA-15, comparable with

(14) Jentys, A. *Phys. Chem. Phys.* **1999**, *1*, 4059.

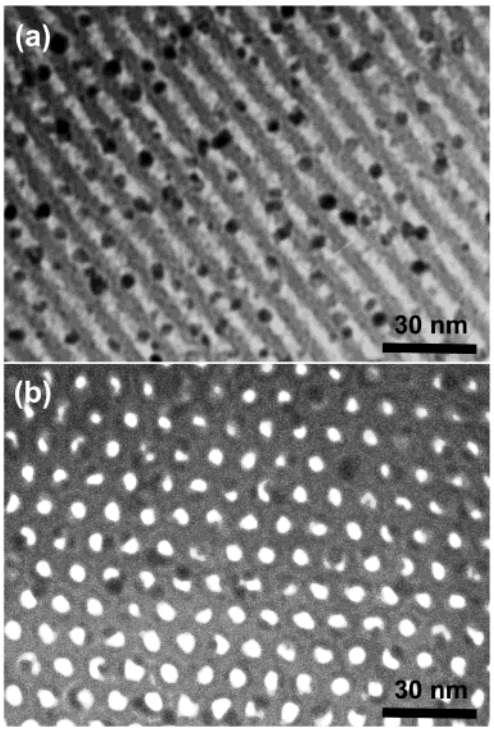

Figure 3. TEM images of Pt/SBA-15 viewing normal to the pore axis (a) and along the pore axis (b) of host SBA-15.

the results of in-situ XAS measurements. The distinct shape of Pt nanoparticles may derive from the electrostatic interaction between positively charged surface PTA groups and anionic Pt complexes, which tends to "pull" the reduced metal onto the pore surface of SBA-15 during reduction. After decomposition of surface PTA groups, Pt forms disk-shaped nanoparticles in the channels of SBA-15.

In the small-angle region of PXRD (Figure 4a), the calcined SBA-15 exhibits intense diffraction peaks, characteristic of a two-dimensional hexagonal ($p6mm$) structure with d_{100} spacing of ca. 9.2 nm. After rehydration and functionalization, the overall pore structure was retained, indicated by the appearance of high-ordered reflection peaks of the sample. However, the PXRD pattern of Pt/SBA-15 composite shows the decrease in peak intensity, especially for (110) and (200) reflections. This is probably due to the difference on the scattering contrasts of the pores and the walls, and to the formation of nanostructured Pt inside the channels of SBA-15 as in the case of MCM-41.[12] In the wide-angle region of PXRD, Pt/SBA-15 exhibits four distinct peaks contributed by Pt metal (Figure 4b). These peaks are very broad and weak, indicating the nanocrystalline nature of Pt in the composite. It also suggests that no large Pt particles outside the host SBA-15 were formed during the reduction process, as large particles would give intense and sharp diffraction signals and dominated the resulting diffraction pattern of the composite. The average Pt particle size was estimated to be 2.3 nm, from the peak width of Pt(111) reflection by using Scherrer's equation with a spherical model for approximation.[15] Once the Pt particles are reductively formed at 573 or 673 K, they are thermally stable up to

(15) Cullity, B. D. In *Elements of X-ray Diffraction*; Addison-Wesley: London, 1978; p 101.

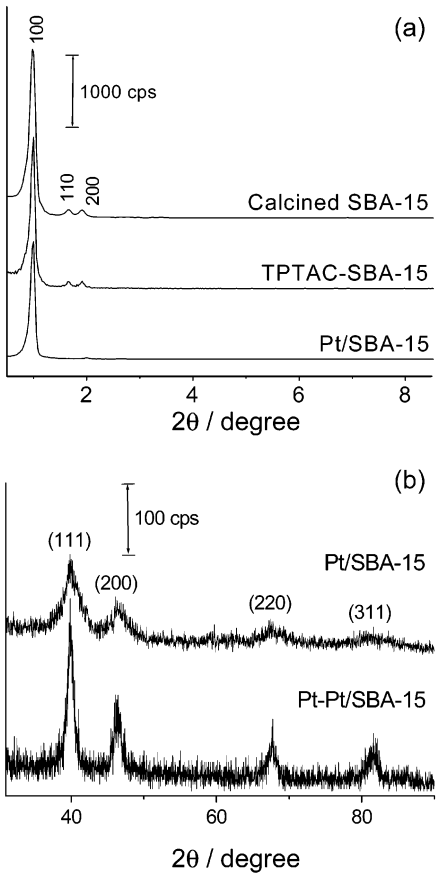

Figure 4. (a) Small-angle PXRD of calcined SBA-15, TPTAC−SBA-15, and Pt/SBA-15. (b) Wide-angle PXRD of Pt/SBA-15 and Pt−Pt/SBA-15.

773 K without any observable diffusion or change in shape.

Preparation and Characterization of Pt−Pt/SBA-15. The surface PTA functional groups of Pt/SBA-15 composite after reduction at 423 K remain on the pore surface of host silica and can be used for secondary incorporation with H_2PtCl_6, to increase the Pt content from ~8 to 12 wt % on Pt−Pt/SBA-15 composite. The additional Pt loading in the second incorporation cycle is less than that in the first incorporation cycle, which may be due to partial decomposition of PTA groups during the first heat treatment, as well as the hindrance of existing Pt nanoparticles in the channels of the composite. The estimated average Pt particles size from the PXRD peak width of Pt(111) reflection on Pt−Pt/SBA-15 (Figure 4b) was 4.0 nm, which is larger than that on Pt/SBA-15 composite (2.3 nm). Again, no obvious anisotropy of Pt nanoparticles in Pt−Pt/SBA-15 was detected.

Figure 5 shows the TEM images of Pt−Pt/SBA-15 composite. The Pt nanoparticles are, on average, 3.5 nm in size with irregular shape. The Pt nanoparticles in Pt−Pt/SBA-15 are larger than those in Pt/SBA-15, with slightly higher density of the particle number in the channels. This suggests that upon heat treatment in hydrogen flow, the reduced Pt derived from secondary incorporation tend to aggregate on the surface of existing Pt nanoparticles, instead of form individual small Pt nanoparticles in the channels of SBA-15. In other words, the existing Pt nanoparticles may serve as the nuclei for further incorporation. This demonstrates that

Table 2. Physicochemical Properties of Selected Samples[a]

sample	S_{BET}/m^2g^{-1}	V_t/cm^3g^{-1}	V_{meso}/cm^3g^{-1}	V_{micro}/cm^3g^{-1}	D_{BJH}/nm	d_{100}/nm	Pt particle size[b]/ nm	
SBA-15	553	0.71	0.59	0.06	5.9	9.2		
Pt/SBA-15	469	0.54	0.47	0.02	5.3	9.2	2.0	2.3
Pt−Pt/SBA-15	415	0.46	0.39	0.02	5.2	9.1	3.5	4.0

[a] S_{BET}, BET specific surface area; V_t, total pore volume; V_{meso}, mesopore volume; V_{micro}, micropore volume; D_{BJH}, pore diameter calculated using BJH method; d_{100}, periodicity of host SBA-15 derived from PXRD. [b] Pt particles size estimated from TEM images (left column) and from the peak width of Pt(111) reflection by using Scherrer's equation with a spherical model (right column).

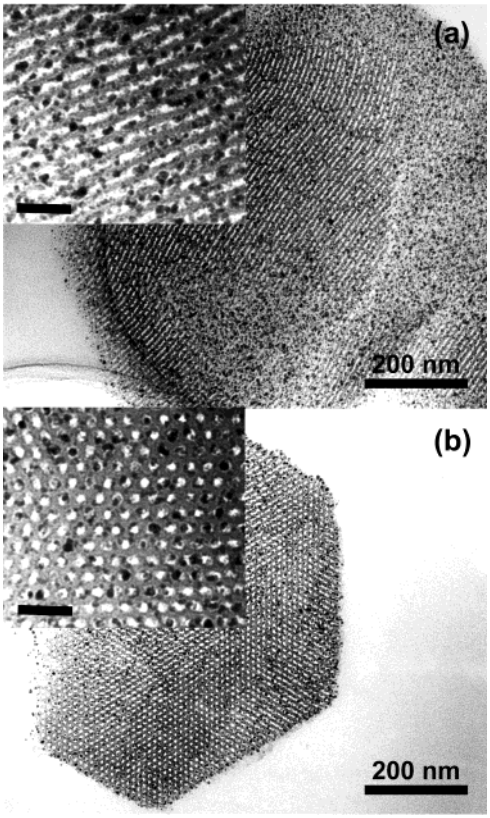

Figure 5. TEM images of Pt−Pt/SBA-15 viewing normal to the pore axis (a) and along the pore axis (b). Insets are the magnifications of the images. Scale bar: 30 nm.

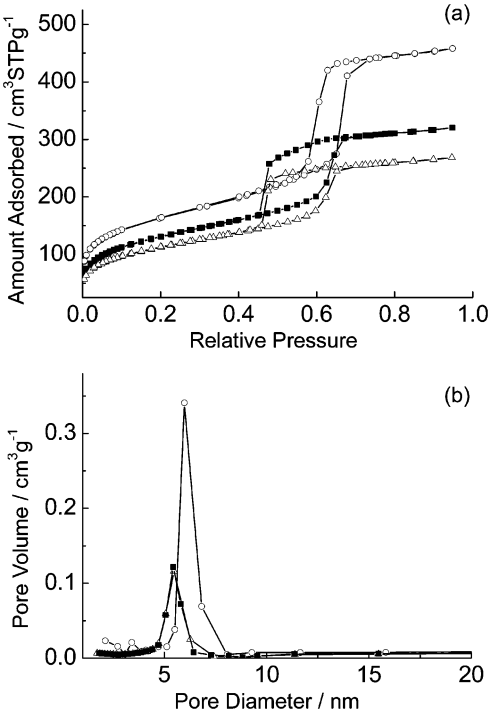

Figure 6. (a) Nitrogen adsorption isotherms of calcined SBA-15 (○), Pt/SBA-15 (■), and Pt−Pt/SBA-15 (△). (b) Pore size distribution of the samples calculated from the desorption branch of the isotherms using the BJH algorithm.

the amount of metal loading as well as the morphology of Pt in host SBA-15 can be rationally controlled through repeating ion-exchange/reduction cycles in the TPTAC−SBA-15 silica host.

Nitrogen adsorption/desorption isotherms for calcined SBA-15 and reduced Pt/SBA-15 or Pt−Pt/SBA-15 are shown in Figure 6. Table 2 summarizes the results of N_2 adsorption analyses, PXRD and TEM observations. The isotherms feature hysteresis loops with sharp adsorption and desorption branches in the P/P_0 range of 0.4∼0.7, indicating a narrow mesopore size distribution (Figure 6b). After the first cycle of Pt incorporation (Pt/SBA-15), the total pore volume (V_t) and mesopore volume (V_{meso}) decrease from 0.71 to 0.54 cm^3/g and from 0.59 to 0.49 cm^3/g, respectively, with a slight decrease of the average pore size (D_{BJH}) from 5.9 to 5.3 nm. This suggests that most of the nanometer-scaled void space of the host silica is open, although a small portion of the channels may be stuck by the Pt nanoparticles. The space is important for guest molecules to diffuse into the host silica, and to contact Pt nanoparticles for reactions to proceed. Secondary Pt incorporation (Pt−Pt/SBA-15) further reduces the mesopore volume to 0.39 cm^3/g. The sorption behavior of the composites is in good agreement with TEM and PXRD characterizations.

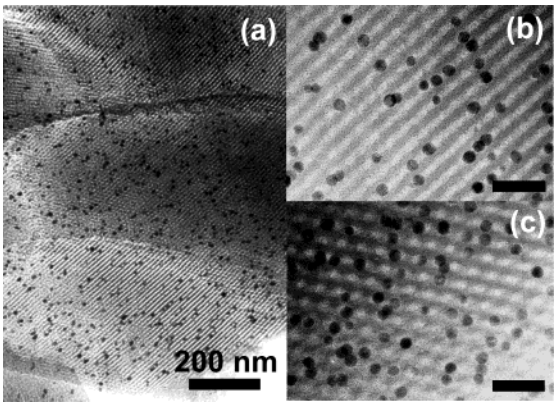

Figure 7. (a) TEM image of Au/SBA-15. (b) and (c) Magnifications of the image. Scale bar: 30 nm.

Preparation and Characterization of Au/SBA-15 and Pt−Au/SBA-15. The same procedure can be applied for synthesis of Au nanoparticles in TPTAC−SBA-15. Au precursors incorporated in TPTAC−SBA-15 were almost twice amount of that for Pt (Au loading of ∼14 wt % on Au/SBA-15) because the charge carried by $AuCl_4^-$ was −1 instead of −2 by $PtCl_6^{2-}$. Figure 7 shows the typical TEM images of the 423 K reduced Au/SBA-

15 composite. Highly dispersed and uniform Au nanoparticles are observed in the hexagonal channels of SBA-15. Compared with that of Pt/SBA-15, the number density of Au nanoparticles in Au/SBA-15 is lower. Almost all the nanoparticles are spherical in shape and of the same size (∼5 nm), close to the pore size of SBA-15. This may be attributed to the intrinsic properties of the two metals, such as melting point, surface energy, etc.[16] It seems that upon reduction, Au tends to form spherical aggregate in order to maximize its size in the confined space of the channel of SBA-15. PXRD of Au/SBA-15 shows characteristic pattern of Au with face-centered cubic structure. By applying Scherrer's equation, the average particle size of Au is estimated at 5.5 nm from the width of Au(111) reflection signal as well as the peak widths of higher-ordered reflection signals (e.g., Au(200), (220), and (311)), indicating the isotropic property of the Au nanoparticles. The estimated particle size is also consistent with what observed by TEM.

The Au/SBA-15 composite was subjected to further incorporation of Pt by secondary ion-exchange and reduction at 473 K. The resulting bimetallic composite (Pt−Au/SBA-15) contains 14 wt % of Au and 5 wt % of Pt as determined by ICP-AES analysis. The morphology and distribution of the two metals in the host SBA-15 are studied by TEM as shown in Figure 8. Two distinct types of metal nanoparticles were found in the composite: one of ∼5.0 nm in diameter, and the other of ∼0.6−1 nm. Compared with the TEM images of Au/SBA-15, the small nanoparticles in the composite may be recognized to be Pt. Both types of nanoparticles are homogeneously distributed in the channels of SBA-15, and this indicates that the originally existing Au nanoparticles do not hinder the diffusion and ion-exchange of $PtCl_6^{2-}$ in the channels of SBA-15. The low amount of Pt loading in the secondary incorporation is due to partial decomposition of the PTA group during Au reduction, and results in the formation of small Pt particles in Pt−Au/SBA-15. The PXRD pattern of the composite is similar to that from Au/SBA-15, while each reflection signal has a small hump at the high-angle side. The pattern may be considered to be derived from two sets of reflection signals of pure Au and pure Pt, suggesting that no alloy phases were present in Pt−Au/SBA-15(a). The estimated particle sizes of Au and Pt nanoparticles are consistent with TEM observations. To our best knowledge, this is the first report on the preparation of two distinct metal nanoparticles in the same channels of a mesoporous host. These results show that the present preparation method is feasible to synthesize various metal nanostructures with controlled morphology and composition in mesoporous materials.

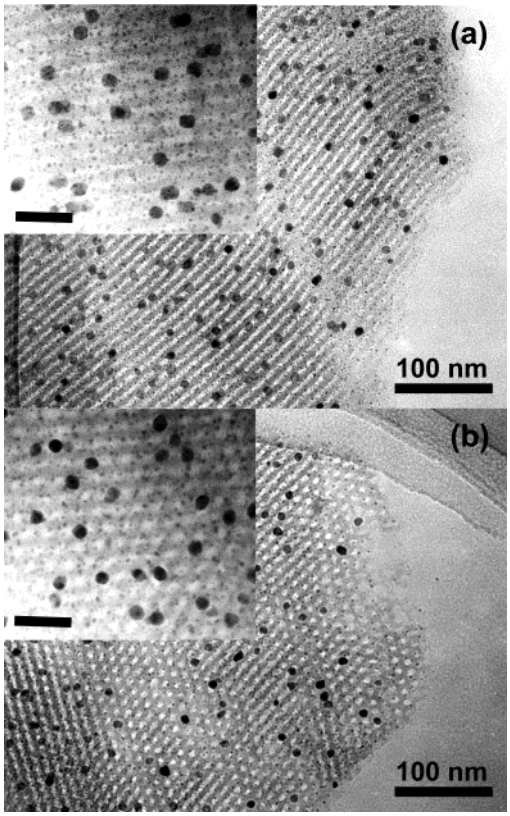

Figure 8. TEM images of Pt−Au/SBA-15 viewing normal to the pore axis (a) and along the pore axis (b). Insets are the magnifications of the images. Scale bar: 30 nm.

Conclusion

In conclusion, the results show that highly dispersed metal nanoparticles can be fabricated in functionalized SBA-15. The metal loading can be controlled via repeating metal incorporation cycles. The morphology of the metal nanoparticles may be affected by the loading amount as well as the intrinsic properties of the metals. Disk-shaped Pt nanoparticles in Pt/SBA-15 are attached on the pore wall of SBA-15 channels, while spherical Au nanoparticles exist in the channels of Au/SBA-15. Subsequent Pt incorporation in Au/SBA-15 generates the coexistence of large Au nanoparticles and small Pt nanoparticles inside the channels of host SBA-15.

Acknowledgment. We thank the National Science Council, Taiwan, for financial support, and the Synchrotron Radiation Research Center for technical support.

CM020822Q

(16) Wang, Z. L. *J. Phys. Chem. B* **2000**, *104*, 1153.